Available online at www.sciencedirect.com
SCIENCE DIRECT
Journal of the European Ceramic Society 26 (2006) 279–287
www.elsevier.com/locate/jeurceramsoc

Sintering and microstructure of rare earth phosphate ceramics $RE PO_4$ with RE = La, Ce or Y

D. Bregiroux[a,b], S. Lucas[a], E. Champion[a,*], F. Audubert[b], D. Bernache-Assollant[a]

[a] *Science des Procédés Céramiques et de Traitements de Surface, Université de Limoges, UMR CNRS 6638, 123, Avenue Albert Thomas, 87060 Limoges, Cedex, France*
[b] *CEA Cadarache, DEN/DEC/SPUA/LTEC, 13108 Saint Paul lez Durance, France*

Received 10 July 2004; received in revised form 9 November 2004; accepted 12 November 2004
Available online 19 January 2005

Abstract

Sintering of rare earth phosphates $RE PO_4$ (RE = La, Ce or Y) was studied using dilatometry. The presence of a secondary rare earth metaphosphate phase $RE(PO_3)_3$ as sintering aid was investigated. It proved to accelerate the densification but it activated fast grain growth, which was very detrimental to the microstructural design of processed ceramics. A temperature of 1400–1450 °C was required to sinter pure $LaPO_4$ and $CePO_4$ ceramics with fine grains. Both compounds behave similar while YPO_4 did not densify even at 1500 °C. The influence of specific surface area of starting powders, temperature and holding time on the sintering rate and microstructures of dense $RE PO_4$ materials is also reported.

Keywords: Rare earth phosphates; Sintering; Grain growth; Microstructure-final; Phosphates

1. Introduction

For some years, a growing interest has been given to rare earth phosphates $RE PO_4$. Synthetic $RE PO_4$ compounds are commonly named after their natural mineral analogue, i.e., monazite for RE = La to Gd or xenotime for RE = Tb to Lu and Y. The first series has a monoclinic crystalline structure[1] while the second has a tetragonal crystalline structure.[2] In the field of ceramic processing, rare earth phosphates have been investigated either for the development of single phased materials or for the elaboration of ceramic–ceramic composites. The main potential applications include host matrices for the immobilization of actinide radionuclide wastes,[3,4] solid protonic conductors[5] and weak fiber–matrix interfaces in ceramic–ceramic composites or thermal protection coatings.[6–8] Whatever the application considered, ceramic processing includes sintering at high temperature. Though the different properties of interest and the thermal behavior have been widely reported, the sintering behavior of these rare earth phosphates has received less attention. Results can be found in the literature for hot pressed[9] or naturally sintered $CePO_4$,[10] which appears to be the most investigated rare earth phosphate. More partial data are available concerning other monazite-type[11–14] or xenotime-type[15] rare earth phosphates.

This study is a continuation of a two part paper devoted to the synthesis and thermal behavior of rare earth phosphate $RE PO_4 \cdot n H_2O$ powders, with RE = La, Ce or Y.[16,17] We demonstrated that low temperature wet chemical routes, which are commonly used to produce synthetic rare earth phosphate powders, led to the formation of a temporary secondary rare earth trimetaphosphate phase during heating. This phase formed at about 950 °C from a reaction between $RE PO_4$ and H_3PO_4 residual species adsorbed at the particle surface:

$$2\,H_3PO_{4(ad)} + RE PO_{4(s)} \rightarrow RE(PO_3)_{3(s)} + 3\,H_2O_{(g)} \quad (1)$$

* Corresponding author. Tel.: +33 555457460; fax: +33 555457586.
E-mail address: champion@unilim.fr (E. Champion).

0955-2219/$ – see front matter © 2004 Elsevier Ltd. All rights reserved.
doi:10.1016/j.jeurceramsoc.2004.11.004

Then, it disappeared by incongruent melting in the 1050–1350 °C temperature range with evolution of P_4O_{10}, leaving pure rare earth phosphate:

$$2\,RE(PO_3)_{3(s)} \rightarrow 2\,REPO_{4(s)} + P_4O_{10(g)} \quad (2)$$

The presence and effects of the rare earth trimetaphosphate during the sintering of monazite powders synthesized by wet precipitation have never been reported, probably because it was not detected. Indeed, it is usually present in very low amount and only in a narrow range of intermediate temperatures (950–1350 °C), which makes difficult its detection. Nevertheless, it may have great consequences on the sintering behavior and properties of materials. The addition of a secondary minor phase as sintering aid is commonly used in ceramic processing in order to enhance densification or to inhibit grain growth.[18,19] But, such a phase may have opposite effects, promoting grain growth or inhibiting densification.[20,21]

This paper is thus devoted to natural sintering of rare earth phosphate ceramics. To this end, thermomechanical analysis (dilatometry) was used. The effect of rare earth trimetaphosphate secondary phase $RE(PO_3)_3$ on the sintering behavior of phosphates was determined and microstructural analyses were performed. The effect of powder preparation was also investigated. Lanthanum phosphate was chosen as reference compound and complementary results on the behavior of cerium and yttrium phosphates are given.

2. Materials and methods

Rare earth phosphate powders were prepared using a wet precipitation process already described.[16] Due to the presence of synthesis residuals adsorbed at the particles surface that form a secondary trimetaphosphate phase $RE(PO_3)_3$ in the temperature range 950–1350 °C, raw powders were heat treated for 1 h at 1400 °C to obtain highly pure $REPO_4$ compounds.[17] Powder X-ray diffraction (XRD) diagrams were recorded using Cu Kα radiation on a $\theta/2\theta$ diffractometer (Siemens D5000, Germany). The crystalline phases were identified from powder diffraction files (PDF) of the International Center for Diffraction Data (ICDD). Powders heated at 1400 °C were well-crystallized and single phased compounds of monoclinic structure for $LaPO_4$ or $CePO_4$ and of tetragonal structure for YPO_4 were obtained (Fig. 1).

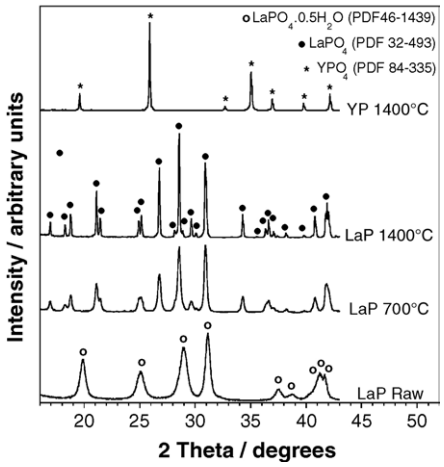

Fig. 1. XRD diagrams of raw and heat treated powders.

In order to increase their specific surface area, the heat treated powders were either ball milled for 5 h with 20 mm alumina balls in an alumina container using a planetary grinder (Fritsch, pulverisette 6, Germany) or attrition milled for a variable time with 1 and 2 mm zirconia balls (50%/50%) in a polyethylene jar (Union Process, model 01 CE, Akron, OH, USA). Specific surface area was measured by the BET method (analyzer Micromeritics ASAP 2010, Norcross, GA, USA), eight points, using nitrogen adsorption at 77 K after degassing the powder at 300 °C. Particle size distribution was measured using a laser analyzer (Cilas 1024, Madison, WI, USA). Preparation, composition and associated references of these powders are summarized in Table 1.

Thermomechanical analysis was performed up to 1400 °C in a vertical dilatometer (Setaram TMA 92, France) to investigate the sintering. Linear shrinkage was measured on 3 mm thick cylindrical pellets using an alumina sensor. The contact load was 0.05 N. The heating and cooling rates were 5 and 10 °C min^{-1}, respectively. Powders were previously compacted in a 10 mm cylinder die under an 80–120 MPa compressive stress. The fraction of the theoretical density of pressed samples ($\tau_{pressed}$, %) was determined from weighing

Table 1
Preparation, composition, specific surface area and reference of rare earth phosphate powders

Ref.	Preparation	Composition
LaP1400-B5	Heated at 1400 °C, ball milled for 5 h	$LaPO_4$
LaP1400-A2	Heated at 1400 °C, attrition milled for 2 h	$LaPO_4$
LaP1400-A5	Heated at 1400 °C, attrition milled for 5 h	$LaPO_4$
CeP1400-A5	Heated at 1400 °C, attrition milled for 5 h	$CePO_4$
YP1400-A5	Heated at 1400 °C, attrition milled for 5 h	YPO_4
LaP Raw	As synthesized powder	$LaPO_4{\cdot}0.61H_2O$ + 2.18 wt.% $La(PO_3)_3$[a]
LaP700-1	Heated at 700 °C	$LaPO_4$ + 1.24 wt.% $La(PO_3)_3$[a]
LaP700-2	Heated at 700 °C	$LaPO_4$ + 2.18 wt.% $La(PO_3)_3$[a]
LaP700-3	Heated at 700 °C	$LaPO_4$ + 3.10 wt.% $La(PO_3)_3$[a]

[a] $La(PO_3)_3$ at 1000 °C, adsorbed hydrogenphosphate in the true composition at 700 °C (see[16]).

and geometrical measurements. The standard deviation was ±1%.

For a comparison, the sintering behavior of lanthanum phosphate powders, either raw, i.e., without any heat treatment, or heat treated at 700 °C for 2 h, and containing H_3PO_4 residuals inducing the formation of various amounts of lanthanum trimetaphosphate (from 1.24 to 3.10 wt.%) during sintering, were also investigated. The amount of $La(PO_3)_3$ was calculated using high temperature thermogravimetry from the weight loss associated with the evolution of P_4O_{10} according to Eq. (2).[16] Typical XRD diagrams of these powders are given in Fig. 1. As already described,[17] the raw materials were hydrated $LaPO_4{\cdot}nH_2O$ ($n \approx 0.6$, rhabdophane-type compounds) while powders heated at 700 °C were anhydrous monoclinic $LaPO_4$ (monazite-type compounds) of a low crystallinity as indicated by the broad diffraction peaks in comparison with those of the same powder heated at 1400 °C. The main characteristics of starting materials are summarized in Table 1.

Additionally, natural sintering of pure $LaPO_4$ monazite was investigated up to 1500 °C to characterize the influence of the thermal cycle on the ceramic properties with the aim of establishing a sintering map. The fraction of the theoretical density of sintered samples (τ_d, %) was calculated from the Archimedean method in water with a standard deviation of ±0.2 or from geometrical measurements with a standard deviation of ±1.

The theoretical density of $REPO_4$ calculated from XRD lattice parameters was assumed to be 5.067, 5.195 and 4.286 for *RE* = La, Ce and Y, respectively. The samples were examined by scanning electron microscopy (SEM, Philips XL 30, The Netherlands). The microstructure of materials was revealed on a mirror polished surface (with 3 μm diamond paste) by thermal etching for 3 min at 25 °C below the sintering temperature. Grain size distribution was determined from SEM images using commercial software (Graphtek, Optibal/Pro-F2.6.1). It was obtained from 500 to 1000 grains of three different images. The grain size or equivalent disk diameter (*D*) was calculated from the measurement of the grain surface (*A*), on the hypothesis of spherical grains, as follows:

$$D = 2\left(\frac{A}{\pi}\right)^{1/2} \quad (3)$$

The "average" grain size (D_{50}) corresponded with 50% of the cumulative frequency. The mean size (G_m) was calculated as the true mean value of the whole measured grain sizes.

3. Results and discussion

3.1. Influence of a metaphosphate secondary phase

The linear shrinkage of lanthanum phosphate pellets in the presence of various amounts of secondary phase $La(PO_3)_3$ is plotted in Fig. 2a and b. Table 2 gives properties of starting and sintered samples. As clearly shown on derivative plots of shrinkage curves (Fig. 2b) linear shrinkage of raw material occurred in three successive steps. The first one, below 500 °C, was due to a lattice volume contraction associated with the dehydration of the initial hydrated rhabdophane-type phosphate. The second one began at about 500 °C and was due to the phase change from the hexagonal structure of dehydrated compound to the monoclinic structure of anhydrous monazite, which is accompanied by a decrease of the molar volume. This shrinkage was continuing up to about 900 °C because of a low crystallinity increase of the monoclinic phase with the temperature. These transformations were detailed elsewhere[17] and do not relate to the actual sin-

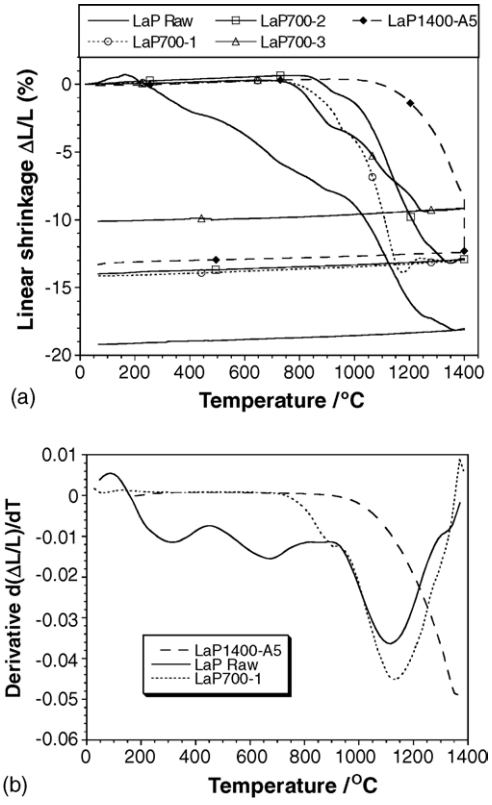

Fig. 2. (a) Linear shrinkage of different lanthanum phosphates vs. the temperature. (b) Derivative plots of linear shrinkage vs. the temperature.

Table 2
Specific surface area, fraction of the theoretical density of pressed and sintered materials at 1400 °C for 1 h

Ref.	S_A ($m^2\ g^{-1}$)	$\tau_{pressed}$ (%)	$\tau_{densification}$ (%)
LaP Raw	78.4 ± 0.2	62	95.5
LaP700-1	30.7 ± 0.3	54	94.9
LaP700-2	31.8 ± 0.3	58	96.0
LaP700-3	32.9 ± 0.5	62	78.0
LaP1400-B5	3.6 ± 0.1	66	71.8
LaP1400-A2	11.0 ± 0.1	63	89.3
LaP1400-A5	17.5 ± 0.2	62	96.7
CeP1400-A5	16.1 ± 0.1	62	97.2
YP1400-A5	28.3 ± 0.2	56	62.2

tering that began with the third step of shrinkage from about 900 °C.

The main differences between raw material and materials initially treated at 700 °C came from the disappearance of the first step of shrinkage and from a shifting of the beginning of the second step above 700 °C. This was due to the calcination at 700 °C that produced the transformation into monazite with a low crystallinity. These steps were not registered on the linear shrinkage curve of pure and well-crystallized monazite initially treated at 1400 °C (LaP1400-A5).

Whatever the material considered, the sintering step began from about 900 °C. Compounds containing lanthanum trimetaphosphate (i.e., raw material or materials heated at 700 °C) had a similar sintering behavior. Densification reached a maximum rate at about 1160 °C. For pure monazite (LaP1400-A5) this maximum was at about 1475 °C (temperature that was determined from a dilatometry experiment performed up to 1600 °C whose plot is not presented in this paper). Thus, it can be hypothesized that the presence of a low amount of lanthanum trimetaphosphate enhances densification of phosphates. Nevertheless, after sintering at 1400 °C for 1 h the densification extent of materials containing up to 2.5 wt.% of lanthanum trimetaphosphate was in the range 95–96% of the theoretical density (Table 2) and it dropped down to 78% with 3.1 wt.% of trimetaphosphate while it reached 96.7% without trimetaphosphate (LaP1400-A5). The microstructure of sintered materials (Fig. 3) gave complementary information to explain this result. Indeed, it appeared that very different materials were processed. With trimetaphosphate (Fig. 3a and b) an important grain growth occurred resulting in grains whose size could reach 50 μm. Some intergranular pores remained in the materials, but a great number of large intragranular pores (up to 5 μm in diameter) were also systematically observed. These microstructures stand in contrast with that of $LaPO_4$ sintered without trimetaphosphate (Fig. 3c). It was homogeneous with fine grains whose size did not exceed 2 μm.

From these results it can be stated that lanthanum trimetaphosphate secondary phase has two opposite consequences on the sintering of lanthanum phosphate.

- on the one hand, it decreases the sintering temperature. It can be remarked that powders containing trimetaphosphate had greater initial surface area ($S_A \approx 32\ m^2\ g^{-1}$) than pure $LaPO_4$ ($S_A = 17.5\ m^2\ g^{-1}$). This parameter could also be taken into account to explain the better sinterability of powders containing trimetaphosphate. Its effect will be detailed in the following subsection;
- on the other hand, it activates strong grain growth. This growth takes place with fast grain boundary migration in which grain boundaries become separated from pores. This phenomenon must be suppressed for reaching high density ceramics because it leads to intragranular pores that inhibit sintering.[18] This detrimental effect on the microstructural design of lanthanum phosphate ceramics appeared particularly important when trimetaphosphate was present in the highest amount of 3.1%, only 78% of the theoretical density being reached.

Considering La_2O_3–P_2O_5 phase diagrams,[22,23] $La(PO_3)_3$ decomposes into $LaPO_4$ with incongruent melting in the temperature range 1050–1235 °C. This melting produces a phosphorus oxide rich liquid and P_4O_{10} gas evolution. The

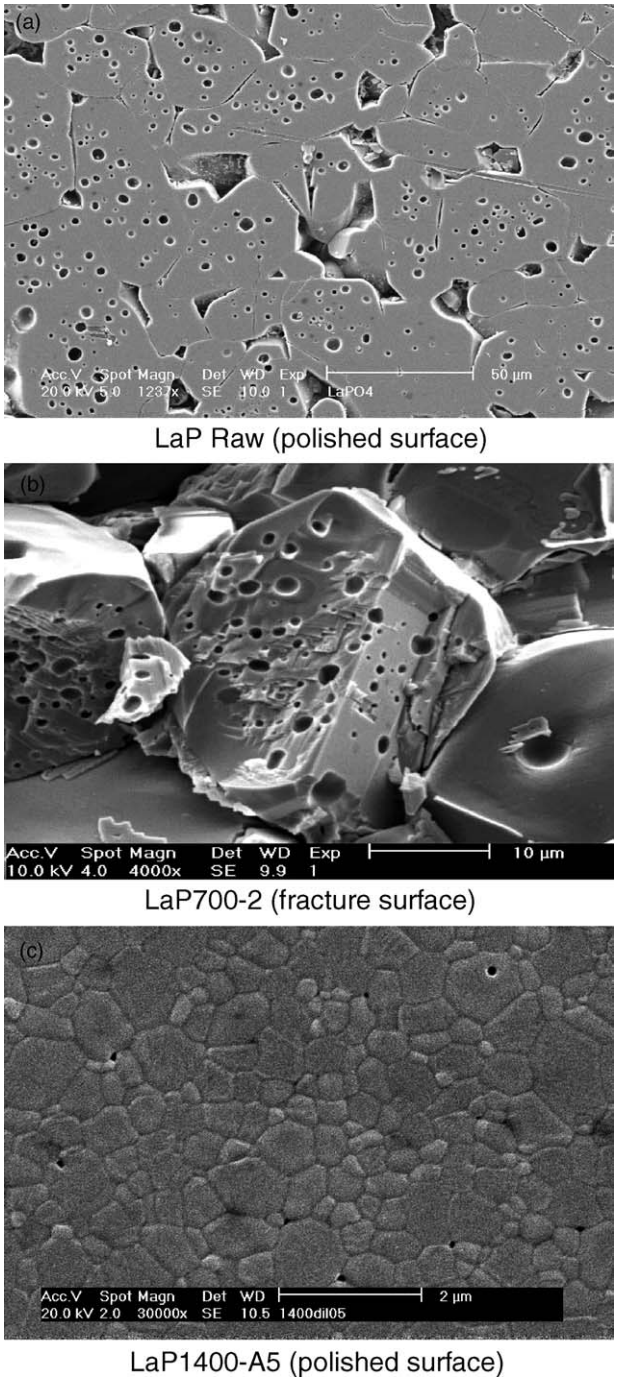

Fig. 3. SEM micrographs of lanthanum phosphate ceramics sintered at 1400 °C for 1 h. (a) LaP Raw (polished surface); (b) LaP700-2 (fracture surface) and (c) LaP1400-A5 (polished surface).

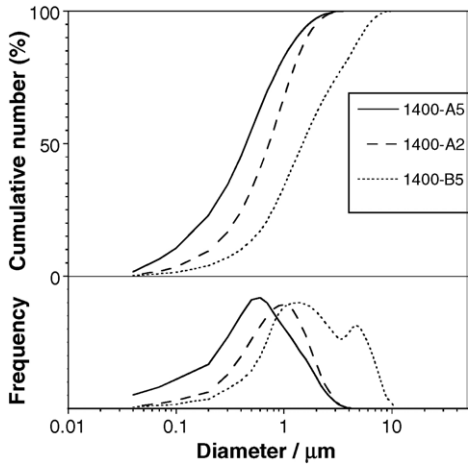

Fig. 4. Particle size distributions of attrition (A) and ball (B) milled $LaPO_4$ powders after calcination for 1 h at 1400 °C.

presence of this secondary liquid phase may explain the decrease of sintering temperature but also grain growth.

3.2. Influence of powder preparation

The influence of powder preparation was investigated using pure $LaPO_4$ powders, i.e., initially heated at 1400 °C for 1 h to remove trimetaphosphate residuals. The specific area being too small after calcination, powder milling was required to increase the reactivity. Fig. 4 shows particle size distribution of ground powders. Attrition milling was much more efficient than ball milling to reduce the grain size of starting powders. After 5 h, powders had a specific surface area of 17.5 $m^2\ g^{-1}$ with an average size $D_{50} = 0.5\ \mu m$. Size distribution was monomodal and narrow which was not the case using ball milling. Increasing the initial surface area of starting powders by grinding induced a decrease of compaction extent after pressing (Table 2) while it enhanced greatly densification after sintering (Fig. 5). Only a surface area of 17.5 $m^2\ g^{-1}$ allowed densification of $LaPO_4$ at 1400 °C up to 96.7% of the theoretical value. In this case, the final stage of sintering was reached, i.e., up to isolated closed pores. For lower surface areas important open porosity remained with densities below 90% of the theoretical value (Table 2, LaP1400-B5 & LaP1400-A2). Thus, surface area of starting materials is an important parameter for sinterability of rare earth phosphates.

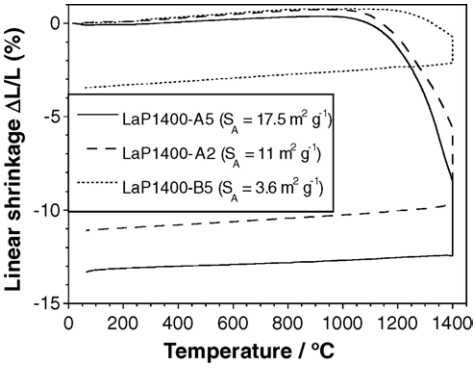

Fig. 5. Linear shrinkage of attrition (A) or ball (B) milled $LaPO_4$ vs. the temperature.

3.3. Influence of thermal cycle

The influence of sintering parameters, i.e., temperature and time, was characterized from pure $LaPO_4$ powder, i.e., heated at 1400 °C for 1 h before the experiments. The characterization included specific surface area, pellets geometrical densification and grain size were measurements. The specific surface area was measured on powder after heating at different temperatures during 5 min with a heating and cooling rate of 10 °C min^{-1}. Geometrical densification of pellets, initially pressed under 80 MPa, was measured after 1 h sintering.

Specific surface area of powder and geometrical densification of pellets versus the temperature are plotted in Fig. 6a. The sintering of monazite-like lanthanum phosphate could be divided in two separated domains. At low temperature, domain (A), specific surface area decreased without densification (Fig. 6b). Such a behavior corresponds to the formation of necks between grains either by gaseous phase

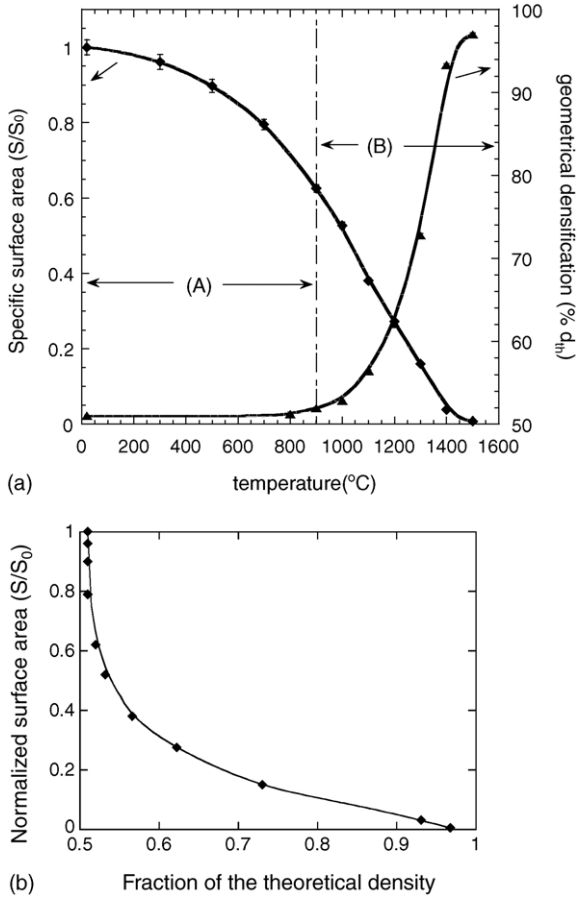

Fig. 6. (a) Specific surface area and geometrical densification of pure $LaPO_4$ vs. the temperature. (b) Specific surface area of pure $LaPO_4$ vs. the fraction of the theoretical density.

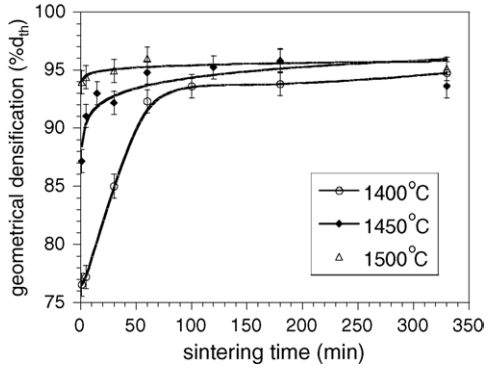

Fig. 7. Geometrical densification of pure $LaPO_4$ vs. the holding time at 1450 and 1500 °C.

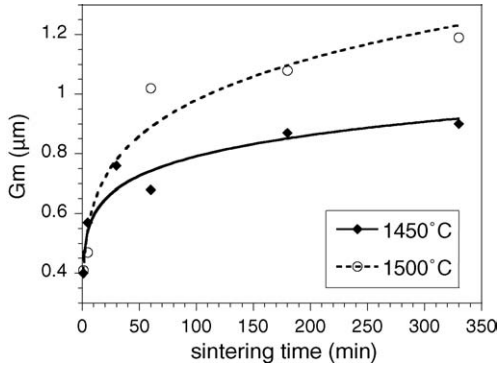

Fig. 8. Mean grain diameter of pure $LaPO_4$ vs. the holding time at 1450 and 1500 °C.

transport or by surface diffusion, mechanisms of matter transport that are known to occur without densification.[24–27] These mechanisms, more particularly surface diffusion, are frequently active in ceramic materials and may lead to important grain coalescence that is detrimental to the sintering.[28] Then, from 900 °C, domain (B) on Fig. 6a, the temperature is high enough to activate lattice or grain boundary diffusion mechanisms, leading to the densification and shrinkage of the pellet (Fig. 6b).

An important result is that the specific surface area is only 60% of its initial value at 900 °C. This means that powder has lost part of its reactivity when densification begins. Since densification kinetics depend on grain size according to a r^{-n} relationship (where r is grain radius and n a constant function of the active diffusion mechanism), it is very important to have a starting powder with a high specific surface area, as it has been shown in Section 3.2. But it is also necessary to reduce grain coalescence at low temperature by using a high rate of heating when possible.

Fig. 7 shows the geometrical densification of pure $LaPO_4$ versus the holding time at 1400, 1450 and 1500 °C. For all of these temperatures, the densification reached a limit of $96 \pm 1\%$ of the theoretical density. 1400 °C appeared too low a temperature to induce significant grain growth, consequently, grain growth was investigated only for temperatures of 1450 and 1500 °C. Mean grain diameter G_m versus

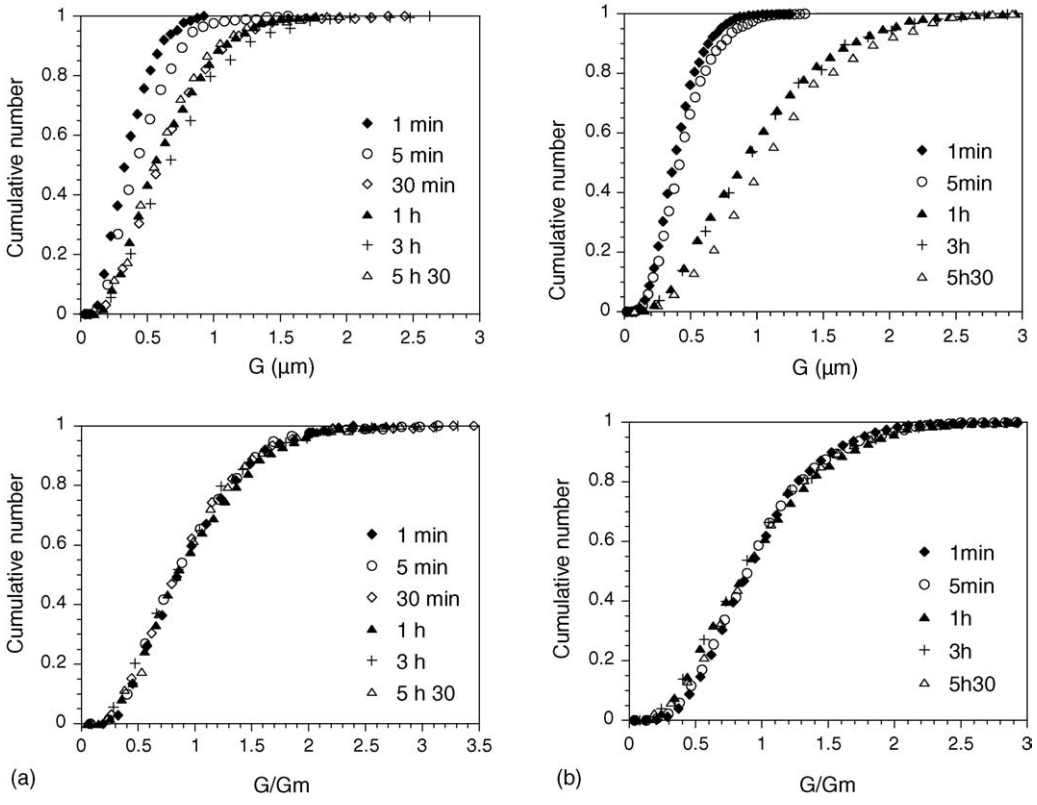

Fig. 9. Grain size distributions of sintered $LaPO_4$ ceramics: (a) 1450 °C and (b) 1500 °C.

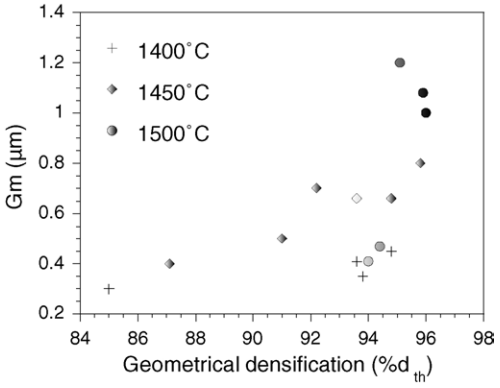

Fig. 10. Sintering map of pure $LaPO_4$.

the holding time at these temperatures is plotted on Fig. 8. It was in the range 0.4–1.2 μm, that is to say within a ratio of three from a treatment of 1 min at 1450 °C for the smallest mean size to 330 min at 1500 °C for the coarsest mean size.

Grain size distributions and normalized grain size distributions after various holding times at 1450 and 1500 °C are plotted on Fig. 9. The normalization consisted in dividing the grain sizes by the mean size for each sintering time. For both temperatures, normalized distributions were strictly identical. This means that microstructures were similar except for a scale factor. This result is indicative of the so-called normal grain growth.

Fig. 10 gives a sintering map of pure $LaPO_4$, i.e., grain size of the material as a function of its densification independently of the sintering temperature. It shows that it is possible to elaborate nearly fully dense ceramics (densification ratio of about 96% of the theoretical value) with controlled microstructure, i.e., having a mean grain size of 0.4–1.2 μm.

3.4. Influence of rare earth element

In view of the results obtained for $LaPO_4$, $CePO_4$ and YPO_4 powders were only attrition milled for 5 h. Fig. 11 gives linear shrinkage of these materials. $CePO_4$ had the same behavior as $LaPO_4$ and the microstructure of sintered samples was identical (Fig. 12a). Such a result was expected because these compounds are very similar. Nevertheless, the temperature of the maximum of sintering rate was lower for $CePO_4$ than for $LaPO_4$ (about 1390 and 1475 °C, respectively), resulting in a slightly higher densification ratio for the same preparation and sintering conditions, i.e., 97.2 against 96.7%, respectively (Table 2). This could be explained by the difference of ionic radii of cations. Ce^{3+} is smaller than La^{3+}: in the nine-fold coordination, ionic radius is 1.196 Å for Ce^{3+} and 1.216 Å for La^{3+}.[29] It is now well established that the monazite structure is the more stable the more the cation is bigger.[30,31] One of the consequences is that the melting point of monazite is decreasing from $LaPO_4$ to $SmPO_4$.[32] The decrease of stability in a structure generally improves ion mobility and, since sintering is due to ion diffusion, it should also improve sinterability.

YPO_4 had a very different behavior; though its initial surface area was slightly higher than those of La or $CePO_4$ (28 $m^2\,g^{-1}$ against about 17 $m^2\,g^{-1}$), the pellets did not sinter. The final density was 62.2% of the theoretical value after 1 h at 1400 °C. SEM observations (Fig. 12b) showed that

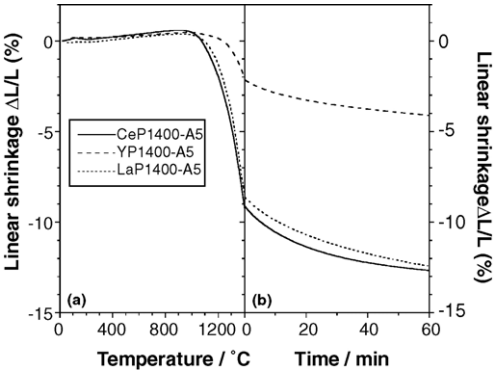

Fig. 11. Linear shrinkage of attrition milled (5 h) *RE*PO_4 vs. (a) the temperature during heating and (b) the time during holding at 1400 °C.

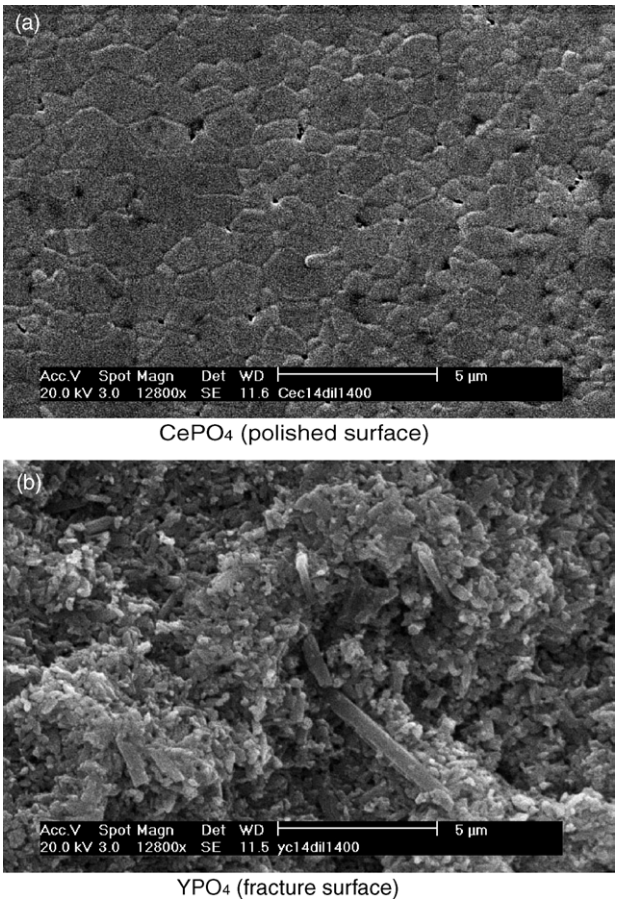

Fig. 12. SEM micrographs of ceramics sintered at 1400 °C for 1 h. (a) $CePO_4$ (polished surface) and (b) YPO_4 (fracture surface).

only the early first stage of sintering occurred, i.e., grain rearrangement and beginning of formation of solid necks between them. This result appears somewhat surprising because YPO_4 has a melting point at 1995 °C, which is below those of $LaPO_4$ and $CePO_4$ (2072 and 2045 °C, respectively). But, this behavior should be explained by the morphological difference between monazite and xenotime particles.16 For YPO_4, the synthesis process led to an important anisotropic crystal growth resulting in needle-like particles while $LaPO_4$ or $CePO_4$ raw powders consisted in small spherical-like particles. This particular morphology of grains can be observed on Fig. 12b and it can be stated that this contributed to the poor sinterability of YPO_4.

4. Conclusion

Due to residual adsorbed species,[16,17] $RE(PO_3)_3$ is present as a minor secondary phase during the sintering of $REPO_4$ synthesized by wet routes. Its effect on the sintering behavior was investigated. Two opposite consequences have been pointed out: $RE(PO_3)_3$ decreases sintering temperature, but it also promotes fast grain growth. this leads to the formation of coarse grains with a high amount of intragranular pores that cannot be resorbed. Consequently, due to its detrimental influence on sintering process, more particularly on the microstructural design of sintered ceramics, $RE(PO_3)_3$ must be eliminated. This can be achieved by heating raw powders at 1400 °C for 1 h.

Specific surface area of powders is also of prime importance in the sintering process of $REPO_4$ and the grinding step has to be considered carefully. For RE = La, nearly fully dense pellets with fine microstructure could be obtained. Monazite-(Ce) had a similar sintering behavior but densification required a slightly lower temperature. YPO_4 do not sinter even at 1500 °C in air. This is due to the needle-like morphology of grains. The densification of YPO_4 requires hot pressing to obtain dense pellets.[33]

References

1. Mooney, R. C. L., Crystal structures of a series of rare earth phosphates. *J. Chem. Phys.*, 1948, **16**, 1003.
2. Hezel, A. and Ross, S. D., X-ray powder data and cell dimensions of some rare earth orthophosphates. *J. Inorg. Nucl. Chem.*, 1967, **29**, 2085–2089.
3. Boatner, L. A., Abraham, M. M. and Sales, B. C., Lanthanides orthophosphate ceramics for the disposal of actinide-contaminated nuclear waste. *Inorg. Chim. Acta*, 1984, **94**, 146–148.
4. Guy, C., Audubert, F., Lartigue, J. E., Latrille, C., Advocat, T. and Fillet, C., New conditionings for separated long-lived radionuclides. *C.R. Phys.*, 2002, **3**, 827–837.
5. Norby, T. and Christiansen, N., Proton conduction in Ca- and Sr-substitued LaPO4. *Solid State Ionics*, 1995, **77**, 240–243.
6. Davis, J. B., Marshall, D. B., Oka, K. S., Housley, R. M. and Morgan, P. E. D., Ceramic composites for thermal protection systems. *Composites: Part A*, 1999, **30**, 483–488.
7. Morgan, P. E. D. and Marshall, D. B., Ceramic composites of monazite and alumina. *J. Am. Ceram. Soc.*, 1995, **78**(6), 1553–1563.
8. Kuo, D. H. and Kriven, W. H., Chemical stability, microstructure and mechanical behavior of $LaPO_4$-containing ceramics. *Ceram. Eng. Sci. Proc.*, 1996, **210**, 257–258.
9. Abraham, M. M., Boatner, L. A., Thomas, D. K. and Rappaz, M., Preparation and compaction of synthetic monazite powders. *Radioactive Waste Manage.*, 1980, **1**(2), 181–191.
10. Hikichi, Y., Nomura, T., Tanimura, Y. and Susuki, S., Sintering and properties of monazite-type $CePO_4$. *J. Am. Ceram. Soc.*, 1990, **73**(12), 3594–3596.
11. Hikichi, Y. and Ota, T., Sintering and properties of monazite-type RPO_4 (R = La, Ce Nd or Sm). *Phosphorus Res. Bull.*, 1996, **6**, 175–178.
12. Hikichi, Y., Ota, T. and Hattori, T., Thermal, mechanical and chemical properties of sintered monazite-(La, Ce, Nd or Sm). *Miner. J.*, 1997, **19**(3), 123–130.
13. Ruigang, W., Wei, P., Jian, C., Minghao, F., Zhenzhu, C. and Yongming, L., Synthesis and sintering of $LaPO_4$ powder and its application. *Mater. Chem. Phys.*, 2003, **79**, 30–36.
14. Terra, O., Clavier, N., Dacheux, N. and Podor, R., Preparation and characterization of lanthanum–gadolinium monazites as ceramics for radioactive waste storage. *New J. Chem.*, 2003, **27**, 957–967.
15. Hikichi, Y., Ota, T., Daimon, K. and Hattori, T., Thermal, mechanical and chemical properties of sintered-type RPO_4 (R = Y, Er, Yb or Lu). *J. Am. Ceram. Soc.*, 1998, **81**(8), 2216–2218.
16. Lucas, S., Champion, E., Bregiroux, D., Bernache-Assollant, D. and Audubert, F., Rare earth phosphate powders $RePO_4{\cdot}nH_2O$ (Re = La, Ce or Y). I. Synthesis and characterization. *J. Solid State Chem.*, 2004, **177**, 1302–1311.
17. Lucas, S., Champion, E., Bernache-Assollant, D. and Leroy, G., Rare earth phosphate powders $RePOO_4{\cdot}nH_2O$ (Re = La, Ce or Y). II. Thermal behavior. *J. Solid State Chem.*, 2004, **177**, 1312–1320.
18. Brook, R. J., Controlled grain growth. In *Treatise on Materials Science and Technology*, ed. F. Y. Wang. Academic Press, 1976, pp. 331–364.
19. Bernache-Assollant, D., *Chimie-physique du frittage*. Editions Forceram, Paris, 1993.
20. Scherer, G. W., Sintering with rigid inclusions. *J. Am. Ceram. Soc.*, 1987, **70**(10), 719–725.
21. Tétard, F., Bernache-Assollant, D., Champion, E. and Lortholary, P., Grain growth kinetics of Li_3PO_4-doped calcium carbonate. *Solid State Ionics*, 1997, **101–103**, 517–525.
22. Park, H. D. and Kreidler, E. R., Phase equilibria in the system La_2O_3–P_2O_5. *J. Am. Ceram. Soc.*, 1984, **67**(1), 23–26.
23. Kropiwnicka, J. and Znamierowska, T., Phase equilibria in the system La_2O_3–Na_2O–P_2O_5 Part I: side system La_2O_3–P_2O_5. *Pol. J. Chem.*, 1988, **62**, 587–594.
24. German, R. M. and Munir, Z. A., Surface area reduction during isothermal sintering. *J. Am. Ceram. Soc.*, 1976, **59**, 379–384.
25. Ruckenstein, E. and Pulvermacher, B., Kinetics of crystallite sintering during heat treatment of supported metal catalysts. *AIChE J.*, 1973, **19**(2), 356–364.
26. Hebrard, J.-L., Nortier, P., Pijolat, M. and Soustelle, M., Initial sintering of submicrometer titania anatase powder. *J. Am. Ceram. Soc.*, 1990, **73**(1), 79–84.
27. Bernache-Assollant, D., Ababou, A., Champion, E. and Heughebaert, M., Sintering of calcium phosphate hydroxyapatite $Ca_{10}(PO_4)_6(OH)_2$ I. Calcination and particle growth. *J. Eur. Ceram. Soc.*, 2003, **23**, 229–241.
28. Raynaud, S., Champion, E., Bernache-Assollant, D. and Thomas, P., Calcium phosphate apatites with variable Ca/P atomic ratio II. Calcination and sintering. *Biomaterials*, 2002, **23**, 1073–1080.

29. Shannon, R. D., Revised effective ionic radii and systematic studies of interatomic distances in halides and chalcogenides. *Acta Crystallogr.*, 1976, **A32**, 751–767.
30. Carron, M. K., Naeser, C. R., Rose, H. J. and Hildebrand, F. A., Fractional precipitation of rare earth with phosphoric acid. *US Geol. Surv. Bull.*, 1958, **1036**, 253–275.
31. Ni, Y., Hughes, J. M. and Mariano, A. N., Crystal chemistry of the monazite and xenotime structures. *Am. Miner.*, 1995, **80**, 21–26.
32. Hikichi, Y. and Nomura, T., Melting temperatures of monazite and xenotime. *J. Am. Ceram. Soc.*, 1987, **70**(10), C252–C253.
33. Lucas, S., Ph.D. thesis. University of Limoges, France, 2002.